Infrared and Raman line shapes for ice Ih. I. Dilute HOD in H_2O and D_2O

Cite as: J. Chem. Phys. **132**, 204505 (2010); https://doi.org/10.1063/1.3430518
Submitted: 05 March 2010 . Accepted: 23 April 2010 . Published Online: 25 May 2010

F. Li, and J. L. Skinner

Infrared and Raman line shapes for ice Ih. I. Dilute HOD in H_2O and D_2O

F. Li and J. L. Skinner[a)]
Department of Chemistry and Theoretical Chemistry Institute, University of Wisconsin, Madison, Wisconsin 53706, USA

(Received 5 March 2010; accepted 23 April 2010; published online 25 May 2010)

Vibrational spectroscopy of ice Ih provides information about structure, dynamics, and vibrational coupling in this important substance. Vibrational spectra are simplified for HOD in either H_2O or D_2O, as in these instances the OD or OH stretch, respectively, functions as a local chromophore. As a first step in providing a theoretical treatment of the vibrational spectroscopy for the fully coupled system (H_2O or D_2O), herein we calculate the infrared and Raman spectra for the isotopically substituted systems. The calculation involves a classical molecular dynamics simulation using a new water model, an initial proton-disordered ice configuration, and *ab initio* based transition frequency, dipole, and polarizability maps. Our theoretical results are in reasonable agreement with experiment, and from our results we provide molecular and physical interpretations for the spectral features. © *2010 American Institute of Physics*. [doi:10.1063/1.3430518]

I. INTRODUCTION

There is continuing interest in understanding the structures and properties of ice, which is one of the most complicated nonmetallic solids, with at least 13 phases with different crystal structures.[1–5] In each structure, the oxygen atoms form a perfect lattice of various symmetries (hexagonal, for example, for ice Ih). On the other hand, the hydrogen atoms are ordered in some structures, but disordered in others. In ice Ih, the stable phase of ice at one atmosphere pressure, and temperatures between 72 and 273 K,[1] and the topic of this paper, the hydrogen atoms are disordered, making this ubiquitous and important solid most interesting indeed. Proton disorder has substantial effects on ice properties, such as density, entropy, heat capacity, dielectric constant, and so on,[1,6–9] and so it is important to characterize it in the various phases. To this end, neutron scattering experiments with isotope substitution[10] have proven to be useful.

Vibrational spectroscopies, both infrared (IR) and Raman, are also useful for probing structure and dynamics in ice. Much effort has focused on the OH stretch region, which is particularly informative since OH stretch frequencies are very sensitive to local molecular environments. Experiments have been performed on neat H_2O, D_2O, and H_2O/D_2O mixtures, for several different ice phases.[11–22] Most experiments are on polycrystalline samples, although some are on oriented single crystals.[15] Regarding the latter, Raman polarization studies with respect to different crystal axes are especially informative. Many studies also use temperature as an important control variable. IR and Raman line shapes for H_2O or D_2O ice Ih crystals show interesting structure, whose assignments have been controversial.[23–25] In a fully ordered crystal, the vibrational modes would display the symmetry of the crystal, and so the OH stretch modes would be delocalized excitons. In a disordered crystal, however, where the translational symmetry is broken, in general it is not clear to what extent vibrational coupling and excitonic delocalization are important. Nonetheless, for ice Ih, at this point at least there is general agreement that intermolecular vibrational coupling is responsible for many of the features in the OH stretch region, making the situation both complicated and interesting.[25–32]

To avoid these complications of vibrational coupling and delocalization, one can also consider spectra for dilute HOD in either H_2O or D_2O, in the OD or OH stretch region, respectively.[12,13,15–17] In these cases, the OD or OH vibrational chromophore is off resonance, and therefore to a large extent uncoupled, from the other stretches, and so it then functions as a local chromophore. Under these circumstances, the line shapes are considerably simpler, with a single main peak corresponding to the OD or OH stretch. Of primary interest are peak frequencies and line widths as a function of temperature. Raman experiments also show an interesting intensity dependence on light polarization and show evidence of a blue side-band (which is only barely present in the IR experiments). The Raman line shapes are generally narrower than IR line shapes, which is particularly interesting, since the reverse is true for liquid water.[33]

Both conventional and *ab initio* molecular dynamics (MD) simulation techniques have been used to study the vibrational properties of ice.[34–42] From the conventional simulations with rigid water molecules one cannot obtain vibrational spectra (except see below) in the OH (OD) stretch regions, but such results are obtainable from the *ab initio* calculations[34,38,42] (since here the molecules vibrate). Results[34,42] using the classical dipole time-correlation function (TCF) for the IR spectra of H_2O and D_2O ice Ih are in only qualitative agreement with experiment, with the calculated vibrational frequencies being substantially too low. This deficiency is most likely due to the density functional employed in the calculations. It is also known that classical (for the nuclear motion) calculations for high-frequency anharmonic modes (like the OH stretch) tend to *overestimate* experimental vibrational frequencies,[33] in which case it is

[a)]Electronic mail: skinner@chem.wisc.edu.

especially surprising that the calculated frequencies are so low.

Other efforts[27,28,31,32] to calculate OH stretch vibrational spectra of ice are based on the pioneering work of Rice and co-workers.[26,29,30] This work involves a mixed quantum/classical approach in which the OH stretch degrees of freedom are treated quantum mechanically, while the other nuclear degrees of freedom are treated classically. In fact, in this implementation the other degrees of freedom are fixed, in that all low-frequency atomic excursions are ignored, and the proton configurations are determined by the (quenched) disorder. The authors assume a certain model for the OH stretch vibrational Hamiltonian, which is diagonalized to produce the vibrational eigenstates, from which the Raman and IR line shapes are calculated. The main limitations of this approach are the neglect of coupling to the low-frequency vibrational modes of the crystal, and the Condon approximation (such that the OH stretch transition dipole is constant, and thus, for example, independent of the proton configurations).

In this paper, we focus on the case of dilute HOD in both H_2O and D_2O ice Ih. We are not aware of other theoretical studies on this system. The theoretical problem is that of a single isolated chromophore, subject to the quenched disorder of the proton configurations, and coupled to the low-frequency vibrational modes of the crystal. Within the harmonic approximation, a fully quantum-mechanical approach for a chromophore coupled to phonons has been well-developed.[43–51] This approach, supplemented with an average over the quenched disorder of the proton configurations,[52] would presumably lead to an accurate description of the line shapes over the full range of temperatures. Such an approach, however, is complicated by the fact that the relevant spectral density for the low-frequency modes depends, at least in principle, on the proton configuration. A simpler approach involves the mixed quantum/classical formulation, wherein the low-frequency modes are treated classically. In this approach, the quenched proton disorder is prescribed, and for each such configuration a classical MD simulation for rigid molecules is performed.

Within this approach, the remaining theoretical task is to assign a transition frequency, dipole, and polarizability, for the OH (OD) stretch chromophore, for each instantaneous configuration of the surrounding molecules. There are a number of possibilities for these assignments,[53–66] but one that we have pursued recently for liquid water involves transition frequency and dipole "maps."[33,67–77] Within the Born–Oppenheimer approximation, the one-dimensional potential curve for the chromophore's OH (OD) stretching motion, and hence its frequency for the fundamental transition, is a functional of the coordinates of the surrounding molecules. The idea is to replace this very complicated dependence on all of these coordinates, by a much simpler dependence on a collective coordinate, involving all of these atomic coordinates, and to define the collective coordinate and parameterize this dependence from electronic structure calculations on water clusters, in the presence of the point-charge electrostatic environment of surrounding molecules. A convenient and successful choice for the collective coordinate is the electric field, from the surrounding molecules, on the H (D) atom of the chromophore, projected along the OH (OD) bond. A quadratic dependence of the frequency on this electric field then defines the transition frequency map. In a similar manner a map for the transition dipole can also be developed. With these maps, an MD simulation then produces transition frequency and dipole trajectories, from which the absorption line shape can be calculated.[78]

In order to implement the above program, we need to choose a water simulation model. The most straightforward choice would be the SPC/E (simple point charge/extended) model, for which transition frequency and dipole maps have been developed.[69,77] Unfortunately, the freezing point of SPC/E water is 217 K,[79,80] making it inadvisable to use that model to describe ice between 217 and 273 K, which is the very region in which our mixed quantum/classical approximation would be most appropriate. Another choice would be the TIP4P model, but here again its freezing point [230 K (Ref. 80)] is well below the experimental value. Attractive choices might be the newer TIP4P/ice[35] and TIP4P/2005[81] models, which have freezing points of 271 and 249 K, respectively.[80] A disadvantage with these models in terms of vibrational spectroscopy is that in each case the point charges differ, meaning that each model requires the development of new maps. Another new model,[82] developed in our group, involves explicit three-body interactions, with the hope and expectation that it will be robust enough to describe the properties of water at the extremes of the phase diagram. Preliminary studies[83] show that with this model water freezes at about 255 K. In addition, this model involves the TIP4P geometry and charges, so that a map developed for TIP4P water can be used for this model (and any other model with the same geometry and charges).

In this paper, we first develop TIP4P transition frequency and dipole maps for the OH (OD) stretch. We then use these maps, together with MD simulations of our new water model, for a single quenched proton-disorder configuration of ice Ih, to calculate IR and Raman spectra of dilute HOD in H_2O and D_2O at 245 K and lower temperatures. The structure of the paper is as follows. In Sec. II we outline our calculation procedure, and in Sec. III we provide our theoretical results, for both single crystal and polycrystalline ice Ih, and compare to experiment. In Sec. IV we present a discussion interpreting our results, and in Sec. V we conclude.

II. CALCULATION OF LINE SHAPES

A. Mixed quantum/classical approach

Both IR and Raman line shapes can be written in terms of quantum TCFs. In the case of IR, if the electric field of the excitation light is polarized in the $\hat{p}$ direction, the linear absorption line shape is[84]

$$I_p(\omega) \propto \mathrm{Re} \int_0^\infty dt e^{i\omega t} \langle \hat{p} \cdot \vec{\mu}(t) \vec{\mu}(0) \cdot \hat{p} \rangle, \tag{1}$$

where $\vec{\mu}(t)$ is the Heisenberg expression for the dipole operator of the system at time t, and the brackets indicate an equilibrium quantum statistical mechanical average. For an isotropic system, of course, the result is independent of $\hat{p}$.

For an oriented single crystal, however, the results do depend on $\hat{p}$. For ice Ih, the set of orthogonal unit vectors are denoted by a, a', and c,[1] and the crystal symmetry shows that $I_a = I_{a'}$.

In the Raman case, the incident beam is polarized in a particular direction, call it $\hat{p}$, and the scattered beam is polarized in direction $\hat{q}$. Similar to the IR line shape, the Raman line shape can be written as[84]

$$I_{pq}(\omega) \propto \mathrm{Re} \int_0^\infty dt e^{i\omega t} \langle \hat{p} \cdot \underline{\alpha}(t) \cdot \hat{q} \hat{p} \cdot \underline{\alpha}(0) \cdot \hat{q} \rangle, \quad (2)$$

where $\underline{\alpha}$ is the polarizability tensor operator for the system. For an isotropic system, the polarized Raman spectrum, when $p=q$, is independent of $\hat{p}$, while the depolarized Raman spectrum is the same for all $\hat{p}$ and $\hat{q}$ such that $\hat{p} \cdot \hat{q} = 0$. For ice Ih, symmetry shows that $I_{aa} = I_{a'a'}$, and that $I_{ca} = I_{ca'}$, thus leaving two independent polarized (I_{cc} and I_{aa}), and two independent depolarized (I_{ca} and $I_{aa'}$) intensities.

Within the mixed quantum/classical approach, for an isolated (in this case OH or OD) chromophore, the IR and Raman line shapes can be written as[72]

$$I_p(\omega) \propto \mathrm{Re} \int_0^\infty dt e^{i\omega t} \left\langle m_p(t) m_p(0) e^{-i\int_0^t d\tau \omega(\tau)} \right\rangle e^{-t/2T_1}, \quad (3)$$

$$I_{pq}(\omega) \propto \mathrm{Re} \int_0^\infty dt e^{i\omega t} \left\langle a_{pq}(t) a_{pq}(0) e^{-i\int_0^t d\tau \omega(\tau)} \right\rangle e^{-t/2T_1}, \quad (4)$$

where $\omega(t)$ is the chromophore's fluctuating transition frequency, $m_p(t)$ is the laboratory-fixed p-component at time t of the chromophore's transition dipole, $a_{pq}(t)$ is the pq-component at time t of the transition polarizability, and T_1 is the excited state lifetime.

B. ES/MD approach and new frequency map

In the above formulae, one sees that from the trajectory of the fluctuating transition frequency and the components of the transition dipole and polarizability, one can calculate IR and Raman line shapes. As discussed in the Sec. I, we have been using frequency and transition dipole maps in order to determine these trajectories. The latest versions of the maps were developed[69,77] for the SPC/E simulation model.[85] As discussed in the Introduction, in this work we will use our new three-body model,[82] whose molecular geometry and charges are identical to the TIP4P model. For this model we will need new maps. Our general approach is to try to develop robust maps, that, for example, could be used for any water model with the same molecular geometry and charges, the idea being that the representative configurations used to parameterize the map are not all that different. A more drastic assumption is that we can use a map parameterized for one water phase, to describe another (even though the representative clusters now would be quite different). As an example, we have used the maps parameterized for bulk liquid water, for the water liquid/vapor interface.[73,75] And, even though configurations with free-OH groups were not present in the bulk liquid configurations, the results were quite satisfactory in comparison with experiment. Therefore, our approach here is to develop maps for the standard TIP4P model in liquid water, and then use these maps for our new model in ice.

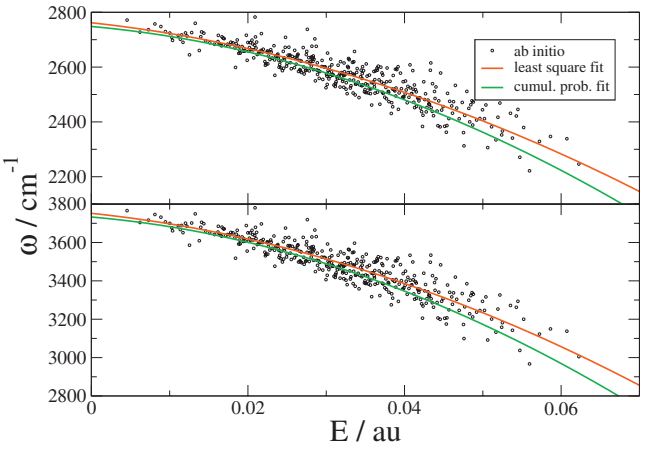

FIG. 1. Calculated OD and OH stretch frequencies, ω, for HOD/H_2O (top panel) and HOD/D_2O (bottom panel) clusters, vs electric field E. Circles are *ab initio* calculations, solid red lines are least-squares quadratic fits, and green lines are fits from the cumulative distributions (see text).

Following the ES/MD (electronic structure/molecular dynamics) approach originally developed by Corcelli *et al.*[68] and most recently implemented by Auer *et al.*,[69] approximately 1700 clusters are generated from an MD simulation of TIP4P water at 300 K. One first selects, at random, an H atom in a given configuration to define the bond of interest. Any molecule having its oxygen atom within 4 Å of this hydrogen is explicitly included in the cluster, and any molecule having its oxygen within 7.831 Å (but larger than 4 Å) of this hydrogen is included through its TIP4P point-charge representation. This is repeated every 500 fs in the course of the simulation until one has the required number of clusters. Electronic structure single-point energy calculations on these clusters of explicit water molecules surrounded by point charges are performed at the B3LYP/6-311++G** level using the GAUSSIAN 03 software package.[86] To calculate the OH stretch frequency for HOD in D_2O, the HOD molecule is treated as an H–OD pseudodiatomic, and the H–OD bond is stretched, keeping the HOD center of mass and orientation fixed, to generate the one-dimensional Born–Oppenheimer curve. The 1–0 transition frequencies are calculated using a discrete variable representation (DVR) scheme.[87] When this procedure is applied to an isolated gas-phase HOD molecule, it yields an OH frequency of 3683 cm^{-1}, slightly below the experimental number of 3707 cm^{-1}.[88] To compensate for this, all calculated frequencies are scaled by 1.0065. For the same set of clusters, this procedure was repeated for HOD in H_2O, now focusing on the D–OH stretch. The OD frequency for the isolated molecule is 2712 cm^{-1}, slightly below the experimental number of 2727 cm^{-1}, and so the calculated frequencies were scaled by 1.0055. These calculated frequencies are shown as the points in Fig. 1.

As in the past, we correlate these frequencies with the component of the electric field parallel to the OH bond, evaluated at the H atom, from the TIP4P point-charge representation of *all* water molecules in the cluster surrounding the HOD molecule. The frequencies are plotted versus this

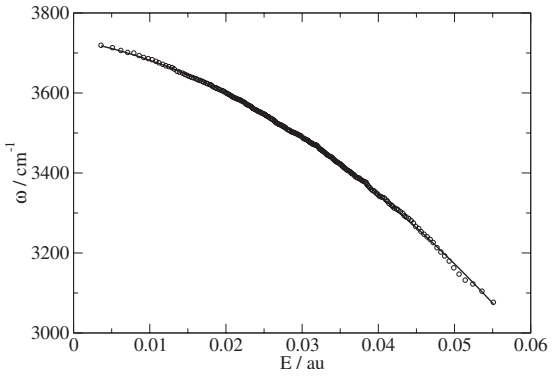

FIG. 2. Numerical solution to the map, from the cumulative histogrammed distribution, for HOD/D_2O. Also shown is the best quadratic fit.

electric field in Fig. 1, and one sees a rough quadratic dependence. In the past, we determined the frequency map by finding the best three-parameter quadratic fit of the frequency as a function of field. The best fits for both the OD and OH stretches are shown as the red lines in the figure, and have root-mean-square (rms) deviations of 41 and 59 cm^{-1}, respectively. One sees a fair amount of scatter from these plots, showing that, in fact, the electric field does not uniquely and precisely determine the frequency.[33,89,90]

The frequencies from the clusters lead to a histogrammed distribution (numbers of clusters with each frequency). On the other hand, from the liquid-state simulation, at every configuration, on every H atom, one can calculate the electric field in exactly the same manner as above, leading to a distribution of electric fields. From the best-fit map, this then leads to a distribution of frequencies. This distribution will be similar, but not the same as (due to the approximate nature of the map, and the finite number of the calculated frequencies) the histogram. In order to calculate an accurate line shape, it would be helpful to obtain the correct (as calculated from the clusters) frequency distribution from the map, which suggests an alternative approach to determine the map. We know the calculated distribution of electric fields from the simulation, $P(E)$, and we know the (histogrammed) calculated distribution of frequencies from the clusters, $p(\omega)$. We then suppose that a map $\omega=\omega(E)$ exists, where (as indicated by the figure) $\omega(E)$ is a monotonically decreasing function of E, which means that low fields correspond to high frequencies, and vice versa. The requirement that the map produce the correct cluster frequency distribution is satisfied by equating the cumulative distributions,

$$\int_{\omega(E)}^{\infty} p(\omega')d\omega' = \int_{-\infty}^{E} P(E')dE'. \tag{5}$$

From this, one can then determine $\omega(E)$ numerically, which is shown in Fig. 2 for HOD/D_2O. These data can be fit very well by a quadratic function, as shown in the same figure, and this quadratic is shown as the green curve in Fig. 1. The rms deviation of these quadratics (47 and 68 cm^{-1} for the OD and OH stretch, respectively), must, of course, be larger than those for the least-square fits (which they are), but only in the latter case is the distribution of frequencies obtained correctly.

TABLE I. Maps for the transition frequencies, matrix elements, and dipole derivatives. Frequencies are in cm^{-1}, while the electric field, matrix elements, and dipole derivative are all in atomic units.

Map	rms error
$\omega_{OH}=3732.9-3519.8E-1.5352\times10^5E^2$	68
$\omega_{OD}=2748.2-2572.2E-1.0298\times10^5E^2$	47
$x_{OH}=0.19318-1.7248\times10^{-5}\omega_{OH}$	3.5×10^{-4}
$x_{OD}=0.16598-2.0752\times10^{-5}\omega_{OD}$	3.3×10^{-4}
$\mu'=0.1622+10.381E+137.6E^2$	0.10

Deciding which map to use is a matter of taste. If one is intent on producing the most accurate frequency for a given field, then one would choose the former (as we have done in the past). If, instead, one considers it most important to produce the correct distribution of frequencies (sacrificing some accuracy for each individual frequency), then one would choose the latter. In this paper, we choose that approach. The quadratic maps for the OD and OH stretches are given in Table I. Note that for $E=0$ these maps gives OD and OH stretch frequencies of 2748 and 3733 cm^{-1}, respectively. On the other hand, the isolated molecule has experimental frequencies of 2727 and 3707 cm^{-1}, respectively. Ideally, our maps would reproduce the gas-phase frequencies when $E=0$, but they do not. We could constrain them to do so, but only at the cost of a larger rms deviation, and so we do not do that herein.

C. Transition dipole and polarizability maps

In the bond-dipole approximation, the projection of the OH (OD) transition dipole moment on the laboratory-fixed p axis is approximately given by[53,67,70,71]

$$m_p = \mu' x\hat{u}\cdot\hat{p}, \tag{6}$$

where μ' is the magnitude of the dipole derivative (the derivative of the dipole of the system with respect to the OH (OD) stretching coordinate), x is the 0–1 matrix element of the OH (OD) stretch coordinate, and $\hat{u}$ is the unit vector in the OH (OD) bond direction. The matrix element is easily calculated within the DVR scheme, and since the ground and excited local-mode vibrational states depend on the solvation environment, so does this matrix element. A simple way to parametrize this dependence is through the local-mode frequency. In Fig. 3, we show linear fits of the calculated matrix elements to the calculated frequencies, for the clusters, for both the OD and OH stretches, and the best-fit equations are given in Table I. The magnitude of the dipole derivative can be obtained from the electronic structure calculations for each cluster, and the results are plotted in Fig. 4 versus the electric field. In the past we have used a linear relationship, but here we assume a quadratic (as shown in the figure), which produces a slightly better fit. The formula for the fit is given in Table I. Note that at $E=0$ this gives $\mu'=0.162$ a.u., which in this case was constrained to be the calculated value for the isolated molecule.

In the bond-polarizability model[91] the pq matrix element of the transition polarizability is given by[91]

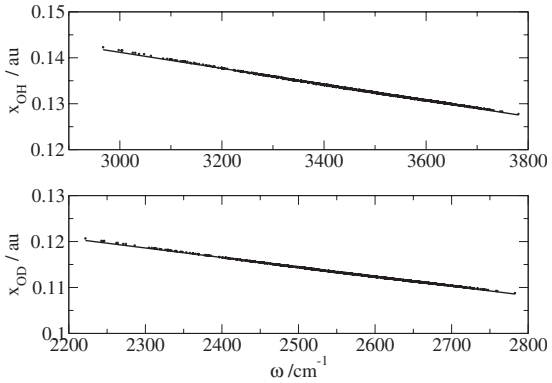

FIG. 3. Calculated matrix element, x (in atomic units), vs frequencies, ω. Top panel is for HOD/D_2O; bottom is for HOD/H_2O. Solid lines are linear fits.

$$a_{pq} = (\alpha'_{\parallel} - \alpha'_{\perp}) x\hat{u} \cdot \hat{p}\hat{u} \cdot \hat{q} + \alpha'_{\perp} x\hat{p} \cdot \hat{q}. \quad (7)$$

Theoretical spectra are determined by $\alpha'_{\parallel}/\alpha'_{\perp}$, which, as in the past,[72] we take to be 5.6, as determined experimentally for ice.[15,92] We briefly explored trying to calculate this ratio theoretically, using electronic structure methods, for different configurations. It is known that for such calculations very large basis sets are needed.[93,94] B3LYP and MP2 calculations with the aug-cc-pVTZ basis set on the isolated molecule give an average transition polarizability ratio of 4.7 and 3.8, respectively, the former of which is similar to that found by Morita and Hynes.[93] Repeated calculations with this basis set on water clusters is prohibitively time-consuming. However, we did perform one B3LYP/aug-cc-pVTZ transition polarizability calculation for one of the OH bonds of the central molecule in an ice-like pentamer, with surrounding molecules (outside the pentamer) replaced by point charges, finding an average ratio of 7.1, which is not far from the experimentally derived value of 5.6 cited above. We also note that for both the isolated monomer and the pentamer cluster, (unlike in the bond-polarizability model) the transition polarizability tensor is not precisely diagonal, and nor are the values in the two perpendicular directions precisely the same.

III. LINE SHAPE RESULTS

A. IR and Raman line shapes for liquid water

Since the maps are parameterized for liquid water, we begin by calculating IR and Raman line shapes for this situation. As discussed earlier, although the maps have been parameterized for the TIP4P model, for the ice calculations we will use our new TIP4P-based model with explicit three-body (E3B) interactions (hereafter called the E3B model),[82] and as mentioned above, will use the TIP4P map (since the geometry and charges are the same). To this end, MD simulations of H_2O in the E3B model were performed using the NVE ensemble with 128 molecules at the experimental density at 300 K using the modified GROMACS PACKAGE 3.3.[95] Periodic boundary conditions were employed, and electrostatic forces were computed using the particle-mesh Ewald technique.[96,97] The equations of motion were integrated with the leapfrog algorithm, using the SETTLE scheme with a 1 fs time step.[98]

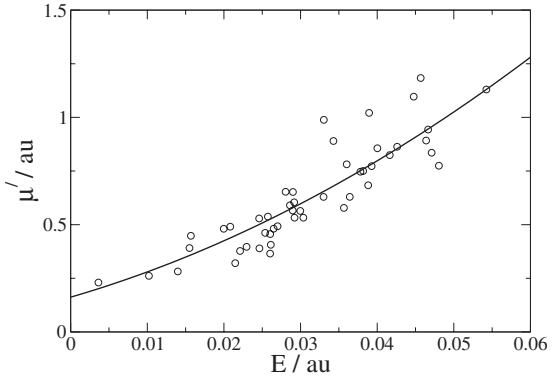

FIG. 4. Calculated dipole derivative, μ' (in atomic units), vs electric field E. Solid line is the best quadratic fit.

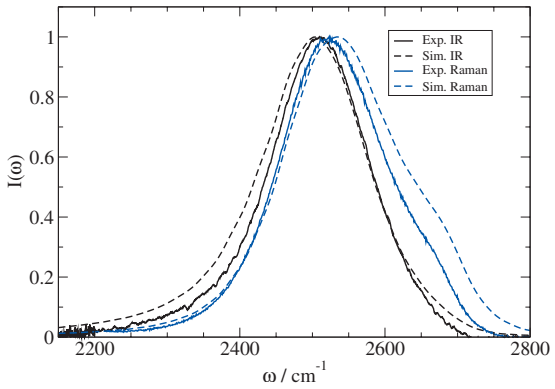

FIG. 5. Experimental (Refs. 102 and 118) and calculated spectra of HOD in (liquid) H_2O at 300 K. All spectra are normalized to have the same peak height.

For HOD/H_2O spectra, at each time step in the simulation we choose one H to be the putative D atom, and calculate the electric field at the atom from the point charges on surrounding water molecules (within the cutoff mentioned above). From this one obtains the OD frequency trajectory, and the trajectories of x and μ'. From the trajectory of the molecule itself one determines the trajectory of $\hat{u}$, which enables one to determine $m_p(t)$ and $a_{pq}(t)$. A time average over the trajectories and an ensemble average over each putative D atom lead to the line shapes. The lifetime T_1 of the OD stretch fundamental is taken to be 1.8 ps.[99–101] The calculated IR line shape, shown in Fig. 5, was obtained as an average over the three Cartesian lab-fixed axes. Agreement with experiment[77] (normalized to have the same peak height) is rather good, for both the peak position and linewidth. For polarized Raman line shapes our calculations are averaged over the three axes, while for the depolarized line shape we averaged over the three orthogonal pairs. The calculated line shapes shown in Fig. 5 are for the unpolarized line shape (which is the sum of the polarized and depolarized spectra), and again, agreement with experiment[102] is quite good. The small blue shift in the Raman line shape (with respect to the IR) and the shoulder at 2675 cm^{-1} are both correctly reproduced by the theory. These results are comparable to those obtained by us earlier for the SPC/E model.[33] For comparison to the ice line shapes that follow, note that these experimental line shapes peak around 2500 cm^{-1}, and have linewidths between 160 and 180 cm^{-1}.

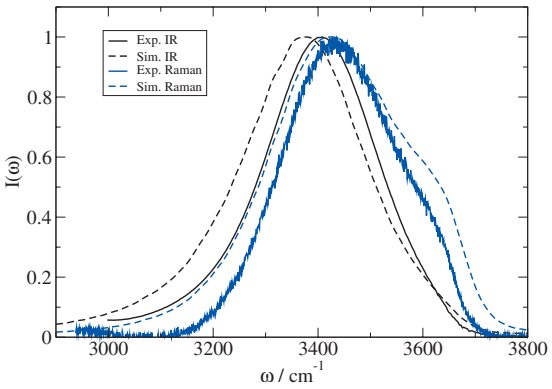

FIG. 6. Experimental (Refs. 102 and 118) and calculated spectra of HOD in (liquid) D_2O at 300 K. All spectra are normalized to have the same peak height.

For the HOD/D_2O spectra, the computational procedure was the same, except we ran a D_2O simulation at the experimental D_2O density, selected putative H atoms, and used OH maps to calculate spectra. The experimental OH lifetime is 700 fs.[103–107] The results are shown in Fig. 6, along with comparison to experiment.[102,108] Agreement is not as good as for HOD/H_2O, but is still satisfactory. Line shapes peak around 3400 cm^{-1}, with linewidths between 250 and 270 cm^{-1}.

B. Raman line shapes for single crystal ice Ih

As discussed above, ice Ih has proton disorder, which would remain fixed on any reasonable simulation time scale. In order to perform a simulation of ice Ih, then, one must generate a specific configuration of proton disorder. The accepted way to do that is to satisfy the "ice rules" (each molecule has two acceptor and two donor hydrogen bonds), while minimizing the total dipole moment of the simulation cell.[37] We used a relatively cubic configuration of 432 molecules generated in such a manner by Hayward and Reimers.[37] We then ran NVE MD simulations for H_2O and D_2O at 245 K, in each case using the experimental lattice constants at that temperature.[1] The OH stretch lifetime in ice is 400 fs.[103] The OD lifetime has not been measured, but assuming the same scaling as in the liquid, we take it to be 1 ps. For HOD in H_2O (D_2O) we averaged over all putative D (H) atoms.

As discussed earlier, for single crystal ice Ih there are two nonidentical polarized Raman line shapes, with intensities I_{cc} and I_{aa}, and two nonidentical depolarized line shapes, with intensities I_{ac} and $I_{aa'}$. These four calculated line shapes for HOD/H_2O at 245 K are shown in Fig. 7, and compared to experimental line shapes at 269 K.[15] Agreement with experiment is excellent, in terms of the peak position, the relative intensities of the four lines, and the shoulder between 2600 and 2700 cm^{-1} in the polarized line shapes. The only significant discrepancy between theory and experiment is in the linewidths, which are somewhat too large in the calculations. Compared to the experimental liquid-state line shapes, we see that the ice line shapes are redshifted and very significantly narrower. Similar results for HOD/D_2O are shown in Fig. 8, with similar agreement between theory and experiment. In this case, notice especially the good agreement in the position and shape of the blue side-band for the polarized spectra.

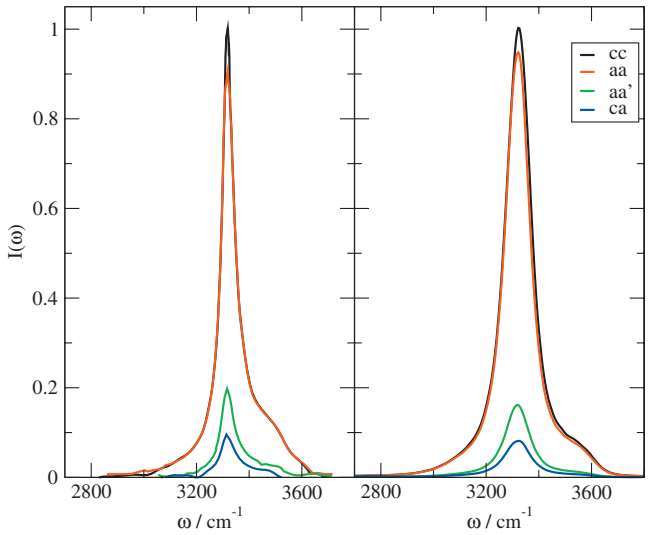

FIG. 7. Experimental Raman spectra for HOD in (single crystal ice Ih) D_2O at 269 K (Ref. 15) (left), and theoretical spectra at 245 K (right). Black lines are *cc* polarized Raman, red lines are *aa* polarized Raman, green lines are *aa'* depolarized Raman, and blue lines are *ca* depolarized Raman. The experimental and theoretical I_{cc} spectra are normalized to have the same peak height.

C. IR line shape for polycrystalline ice Ih

As far as we know, there are no published IR line shapes on single crystal ice Ih, but there are experiments on polycrystalline samples. Assuming that these samples consist of randomly oriented single crystals, it is easy to show that IR spectra can be calculated from an equal linear combination of I_c, I_a, and $I_{a'}$. The calculated IR line shape for HOD/D_2O at 245 K is shown in Fig. 9, and compared to the experimen-

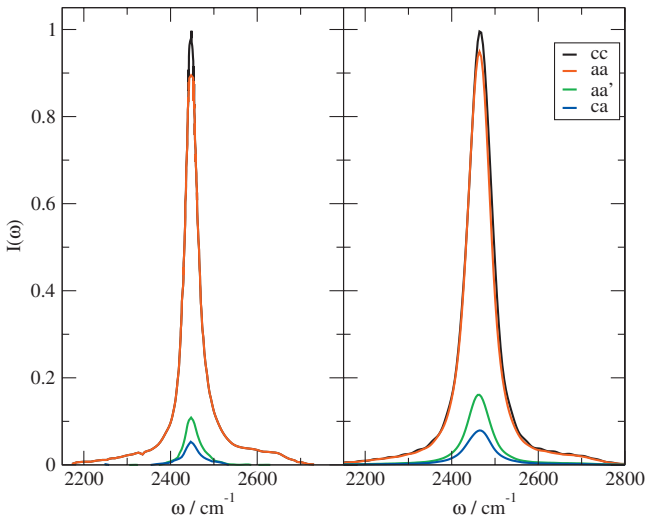

FIG. 8. Experimental Raman spectra for HOD in (single crystal ice Ih) H_2O at 269 K (Ref. 15) (left), and theoretical spectra at 245 K (right). Black lines are *cc* polarized Raman, red lines are *aa* polarized Raman, green lines are *aa'* depolarized Raman, and blue lines are *ca* depolarized Raman. The experimental and theoretical I_{cc} spectra are normalized to have the same peak height.

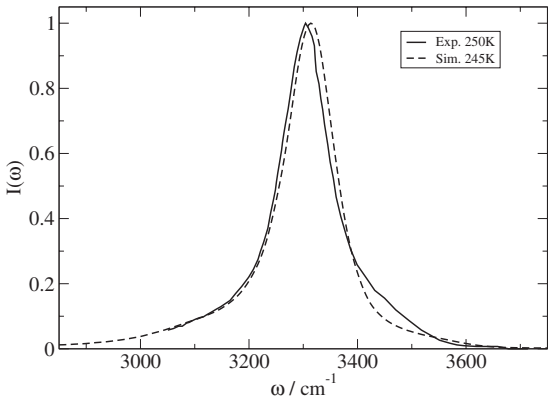

FIG. 9. Experimental IR spectrum for HOD in (polycrystalline ice Ih) D_2O at 250 K (Ref. 109) (solid line), and simulated spectrum at 245 K (dashed line). The spectra are normalized to have the same peak height.

tal result at 250 K.[109] In this case agreement between theory and experiment is excellent both in terms of line position and linewidth. Note that the (experimental) peak position at about 3300 cm^{-1}, is slightly redshifted from the peaks in the Raman spectra, while the linewidth of about 100 cm^{-1} is significantly broader than the Raman linewidths.

In fact, IR line shapes have been measured between 70 and 273 K, for polycrystalline HOD/D_2O, and the results for linewidths and peak positions are shown in Fig. 10. The linewidth seems to decrease monotonically with temperature, but perhaps levels off at about 65 cm^{-1} at low temperature (although the one experimental point at 70 K is considerably lower). The peak position monotonically redshifts as temperature is lowered. We have performed simulations at 125 K and at 1 K for HOD/D_2O, in each case using the experimental lattice constants. Our results for the linewidth and peak position are shown in Fig. 10. The values at 125 K are in good agreement with experiment. There are no experiments at 1 K [and, in fact, ice Ih is probably not the most stable form at 1 K (Ref. 1)]. The theoretical peak position is consistent with the experimental extrapolation, and the theoretical linewidth is about 70 cm^{-1}.

IV. DISCUSSION

Given the relatively good agreement between theory and experiment, we can now try to understand some features of

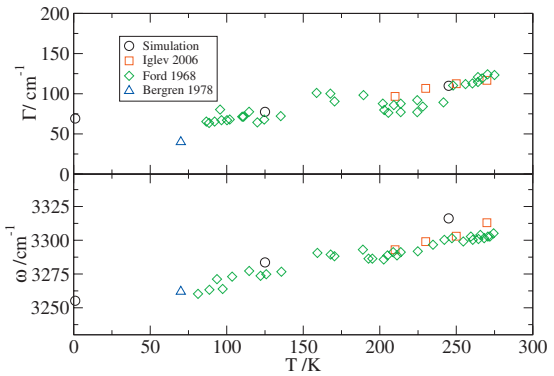

FIG. 10. Experimental and simulation IR linewidths (Γ) and peak positions (ω) for HOD in (polycrystalline ice Ih) D_2O as a function of temperature.

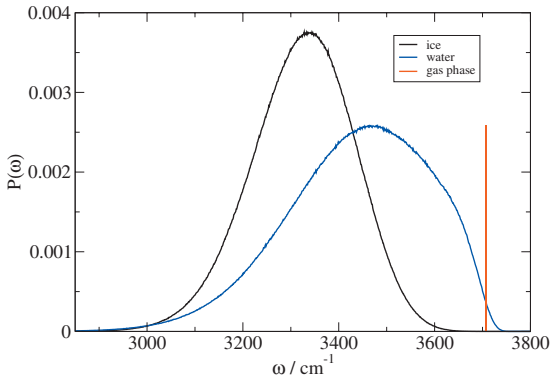

FIG. 11. Calculated frequency distributions for HOD/D_2O. The solid black line is for ice at 245 K, and solid blue line is for water at 300 K. The red line indicates the value of the gas-phase frequency.

both. For example, why are the ice line shapes so much narrower than the liquid line shapes? Why are they redshifted from the liquid line shapes? Why are the IR line shapes redshifted from the Raman line shapes in ice? Why are the Raman line shapes in ice narrower than the IR line shapes? What is the origin of the shoulder on the blue side of the polarized Raman ice line shapes? What is the origin of the residual breadth at 1 K?

We begin by discussing the origins of the differences between the liquid water and ice spectra. To this end, it is useful to consider the calculated frequency distributions in the two cases, for example, for HOD/D_2O, as shown in Fig. 11. The red line is the position of the gas-phase frequency. The liquid-state frequency distribution is very broad, redshifted, and asymmetrical. We can understand the liquid IR spectrum (at 300 K), as an evolution from this frequency distribution, to a spectral density (squared-transition-dipole-weighted frequency distribution) that is further redshifted and narrowed (due to non-Condon effects), to the line shape that includes the additional effects of motional narrowing (due to the fast dynamics of the frequency fluctuations).[33,71,110] Raman spectra are similar, but non-Condon effects are much less important. This kind of analysis shows that, for HOD in liquid D_2O, motional narrowing reduces the IR linewidth by 10% or 15%.[110] The IR spectrum for the liquid is redshifted compared to the Raman spectrum due to non-Condon effects (since the transition dipole is larger on the red side of the line), and the blue shoulder in the Raman spectrum is due to the presence of HOD molecules with broken hydrogen bonds.[33,110]

One sees that the frequency distribution for ice (at 245 K) is more redshifted, narrower, and more symmetrical than that for water. The distribution is redshifted because there is more, stronger, hydrogen-bonding in ice (and hydrogen bonds generally correspond to more redshifted lines), it is narrower because the distribution of local environments is narrower (because the solid is more ordered than the liquid), and it is more symmetrical because the constraints of the ice lattice do not allow for unusual configurations. One can understand the ice spectra in a similar way as above, except that non-Condon effects are less important, since the frequency distribution is already substantially narrower. Still, IR spectra are weakly redshifted compared to Raman spectra because of

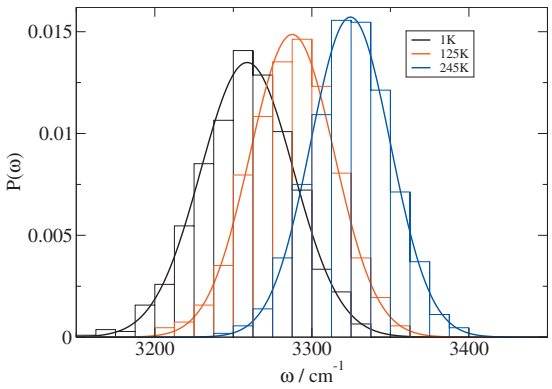

FIG. 12. Histogrammed distribution of time-averaged frequencies for HOD/D_2O in ice at 245, 125, and 1 K. The solid lines are the best Gaussian fits.

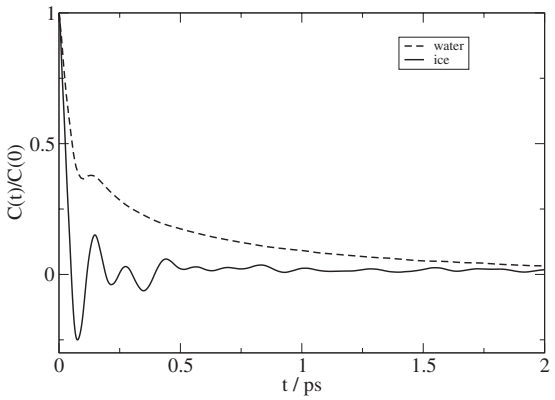

FIG. 13. Frequency-frequency TCFs for HOD/D_2O. Dashed line is for liquid water (300 K), and solid line is for ice (245 K).

these non-Condon effects. In ice, motional narrowing must be much more significant, since the width of the frequency distribution in Fig. 11 is about 250 cm^{-1}, whereas the theoretical linewidths are on the order of 100 cm^{-1}.

One must also consider the effect of the quenched proton disorder, which will not be narrowed on any spectroscopic time scale. To quantify the latter, we calculate the time-averaged frequency for each of the 864 putative OH chromophores. Each of these will be different because each has a different quenched proton disorder environment. In Fig. 12 we plot the histogrammed distribution of these time-averaged frequencies at 245 K, which appears to be more or less Gaussian, and, indeed, it can be fit well by a Gaussian, as shown in the figure. The width of this distribution is about 65 cm^{-1}. This, then, makes a modest contribution to the frequency distribution, but a dominant contribution to the linewidth. In the same figure we also plot the histogrammed distributions of time-averaged frequencies at 125 and 1 K, together with Gaussian fits. These distributions are weakly temperature dependent, becoming broader and more red-shifted as temperature decreases, due to the changing density. At 1 K the full-width at half-maximum of this distribution is about 70 cm^{-1}, consistent with the low-temperature residual linewidth.

To consider specifically the effect of motional narrowing, we first calculate the average transition frequency TCF in ice, and compare to that for the liquid. For the liquid, the time average of each putative OH chromophore is the same, and so when calculating the average frequency TCF, we subtract off the same average from each frequency. For ice, however, since the time-averaged frequency is different for each chromophore (as discussed above), we need to subtract off a different average in each case. Thus, the TCF for the i^{th} chromophore is

$$C_i(t) = \langle(\omega_i(t) - \langle\omega_i\rangle)(\omega_i(0) - \langle\omega_i\rangle)\rangle, \tag{8}$$

where $\omega_i(t)$ is the fluctuating frequency for the i^{th} chromophore. These average TCFs for ice (at 245 K) and liquid water (at 300 K), normalized by their initial values, are shown in Fig. 13. The liquid TCF shows a fast initial decay, followed by a slight recurrence at about 145 fs, followed by a decay with a time scale on the order of 1 ps. The recurrence has been assigned to the intermolecular hydrogen-bond stretch motion, and the final decay to hydrogen bond rearrangement dynamics.[54,55,58,59] The initial decay for ice is on an even faster time scale, followed by a distinct recurrence (whose period is roughly the same as in the liquid) with several beats. The recurrence is presumably again due to the hydrogen-bond stretch, and there is no long-time decay since there is no hydrogen-bond rearrangement in ice on this time scale. To get a rough idea of the extent of motional narrowing in ice, one can be guided by the Kubo model.[111] Thus, we characterize the average TCF by its initial value $C(0)=\Delta^2$, and its decay time τ by

$$\tau = \int_0^\infty dtC(t)/C(0). \tag{9}$$

For ice we find that $\Delta=107$ cm^{-1} and $\tau=65$ fs. The dimensionless product $\Delta\tau$ determines the amount of motional narrowing: $\Delta\tau$ is 0.13, indicating that the line shape is well into the motional-narrowing limit.[112,113]

The above suggests that, for example, the *cc* Raman spectra, at 245 K, can be understood as a convolution of Gaussian (since the distribution of average frequencies is more or less Gaussian) inhomogeneous broadening due to the quenched proton disorder, and Lorentzian (since the system is in the motionally narrowed limit) homogeneous broadening due to the thermal fluctuations. To see if this is the case, let us first consider neglecting rotations and making the Condon approximation, so that the line shape becomes

$$I_{cc}(\omega) \propto \mathrm{Re}\int_0^\infty dte^{i\omega t}\left\langle e^{-i\int_0^t d\tau\omega(\tau)}\right\rangle e^{-t/2T_1}. \tag{10}$$

This approximation, compared to the full line shape (from Eq. (4)), is shown in Fig. 14. The reasonable agreement shows that this approximation is satisfactory. To provide a formal justification of the above suggestion, we next perform a cumulant expansion,[78] truncating at second order, and suppose that the frequency fluctuations arise from a sum of independent slow (from the quenched disorder) and fast (from the thermal fluctuations) processes.[113] Assuming that the thermal fluctuations are statistically the same for each chromophore (that is, assuming the existence of a "homogeneous" line shape), within the motionally narrowed limit the line shape is given by[113]

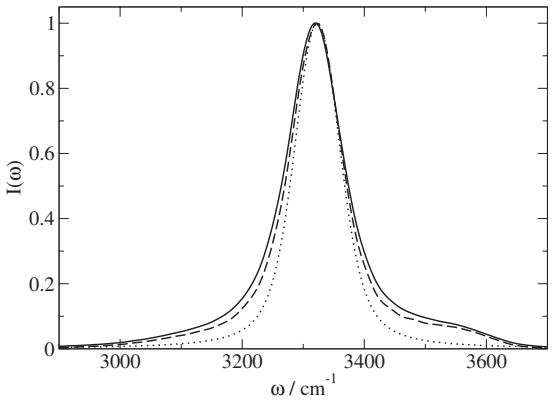

FIG. 14. *cc* Raman line shapes for HOD/D_2O at 245 K. The solid line is the exact result from Eq. (4), the dashed line comes from Eq. (10) (neglecting rotations and making the Condon approximation), and the dotted line is the convolution of inhomogeneous and homogeneous broadening from Eq. (11). The three curves are normalized to have the same peak height.

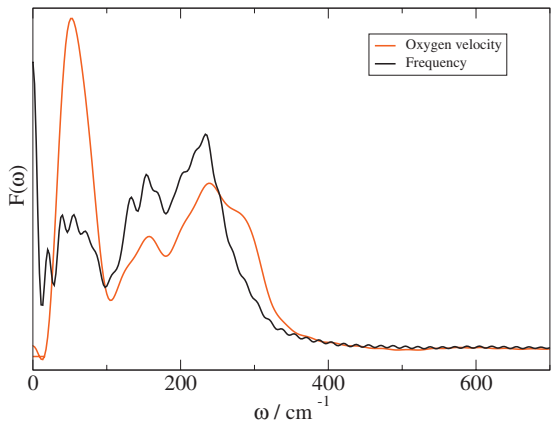

FIG. 15. Fourier transform of the frequency TCF (black line) for HOD/D_2O, and Fourier transform of the oxygen atom velocity TCF (red line).

$$I_{cc}(\omega) \propto \int_0^\infty dt \cos \omega t e^{-\sigma^2 t^2/2} e^{-t/T_2}, \tag{11}$$

where σ^2 is the variance of the distribution of time-averaged frequencies (σ=27.8 cm^{-1}, as given by the Gaussian fit in Fig. 12),

$$\frac{1}{T_2} = \Delta^2 \tau + \frac{1}{2T_1}, \tag{12}$$

and Δ and τ are given above. This approximation to the line shape is also shown in Fig. 14. The reasonable agreement among all three lines in the figure shows that this simple picture is approximately correct.

The next issue involves the origin of the blue shoulder in the (experimental and theoretical) single crystal polarized Raman spectra, which is, for example, between 3500 and 3600 cm^{-1} for HOD/D_2O. Scherer and Snyder have suggested that this is a combination band of the OH stretch and a lattice mode.[15] If this suggestion is correct, from the position of the side-band, one arrives at a lattice mode frequency of about 200 cm^{-1}. The results in Fig. 14, showing the good agreement when neglecting rotations, indicates that this lattice mode is only weakly coupled to rotations, but must be more strongly coupled to OH stretch frequencies themselves. Indeed, one still sees the side-band within the approximation of Eq. (10). Note, however, that the side-band must arise from non-Gaussian fluctuations, since within the second-cumulant approximation the line shape is symmetric.

To investigate further this issue, in Fig. 15 we show the Fourier transform of the average frequency TCF, discussed earlier, and the oxygen velocity TCF. The former shows the low-frequency lattice motions coupled to the OH stretch frequency fluctuations, while the latter shows the low-frequency modes associated with oxygen translation. The oxygen velocity TCF shows a mode at about 60 cm^{-1}, associated in the liquid with the O–O–O bend,[114,115] and a peak at about 230 cm^{-1} associated with the intermolecular hydrogen-bond stretch.[116] On the other hand, the frequency TCF is not very strongly coupled to the O–O–O bend, but is strongly coupled to the 230 cm^{-1} mode. Thus, this mode shows up as the pronounced oscillation at about 145 fs in the frequency TCF in Fig. 13, and as the side-band in the Raman spectrum at about 3560 (=3330+230) cm^{-1}. This side-band is absent in our theoretical IR line shape, and perhaps only weakly present in the experimental IR line shape (in both cases see Fig. 9), presumably as a result of non-Condon effects (since on the far blue side of the line the transition dipole is substantially weaker).

V. CONCLUSION

We have extended our calculations of the vibrational spectroscopy of HOD in liquid water and heavy water into the solid phase. We have used a new water simulation model that freezes near the experimental freezing point, and have developed new frequency and transition dipole maps for this (and related) models. Our proton-disordered configuration for ice Ih is obtained from previous work. We calculate IR and Raman line shapes, for HOD in H_2O and D_2O, for single crystal and polycrystalline ice Ih, at 245 K, and at lower temperatures. Theoretical peak positions are in excellent agreement with experiment, and theoretical linewidths are in fair to excellent agreement. The interesting shoulder on the blue side of the Raman spectra is correctly reproduced by the theory.

Our analysis of these results allows us to provide molecular and physical interpretations for several interesting phenomena. The ice spectra are redshifted from those in liquid water because of stronger and more complete hydrogen bonding in ice. Ice spectra are narrower than those in the liquid, because the distribution of frequencies is narrower in ice, since the solid is more ordered, and the amount of motional narrowing is much more significant in ice. In fact, the spectra can be well understood as a convolution of nearly Gaussian inhomogeneous broadening due to quenched proton disorder, and homogeneous broadening from thermal fluctuations, which is in the motionally narrowed (Lorentzian) limit. Since the spectrum is dominated by the inhomogeneous broadening, it is now clear why the pioneering theoretical work of Rice and co-workers,[26,29,30] which neglects all thermal broadening, is qualitatively correct. We identify

the origin of the blue shoulder as a combination band of OH (OD) stretch and the intermolecular hydrogen-bond stretch.

There are some features that we do not reproduce correctly, namely that the Raman spectra are narrower than IR spectra in ice at the same temperature, and that both IR and Raman spectra at low temperature seem to be narrower than could arise from our model (since our quenched proton disorder leads to a minimum linewidth of about 70 cm^{-1} for the OH stretch, whereas the experimental Raman linewidth[12] at 10 K is as low as 25 cm^{-1}). These discrepancies point to limitations of the model, which may arise from a number of sources, including: the accuracy of the simulation model, the use of a classical simulation model at low temperatures, the correctness of the proton-disordered configuration, the accuracy of the frequency map, the appropriateness of using the frequency map developed for the liquid phase for ice calculations, the accuracy of the bond-polarizability approximation, and the appropriateness of making the Condon approximation for the Raman spectra. In terms of the differences between the IR and Raman linewidths, it seems likely that this is related to possible limitations of the polarizability model. The excess line broadening at low temperatures might be reduced with a frequency map parameterized from ice configurations. Alternatively, it may be that the standard procedure for generating proton disorder does not lead to correct configurations.[9] That is, it may be that ice structure is locally more ordered than what arises from this procedure. These are all interesting questions for future study. Nevertheless, we believe that the calculations described herein show that we have a correct qualitative understanding of the spectra.

The next step, described in a companion paper,[117] is to treat neat H_2O and D_2O ice Ih. Intramolecular and intermolecular vibrational coupling produces significant delocalization of the vibrational states, which in turn leads to interesting and detailed structure in the IR and Raman spectra. Development of coupling maps allows us to calculate vibrational spectra for this significantly more complicated case, and to provide an interpretation for the observed spectral structure.

ACKNOWLEDGMENTS

This work was supported by DOE Grant No. DE-FG02-09ER16110 and NSF Grant No. CHE-0750307.

[1] V. F. Petrenko and R. W. Whitworth, *Physics of Ice* (Oxford University Press, Oxford, 1999).
[2] C. G. Salzmann, P. G. Radaelli, A. Hallbrucker, E. Mayer, and J. L. Finney, Science **311**, 1758 (2006).
[3] Y. Takii, K. Koga, and H. Tannaka, J. Chem. Phys. **128**, 204501 (2008).
[4] M. de Koning and A. Antonelli, J. Chem. Phys. **128**, 164502 (2008).
[5] C. G. Salzmann, P. G. Radaelli, E. Mayer, and J. L. Finney, Phys. Rev. Lett. **103**, 105701 (2009).
[6] C. Knight and S. J. Singer, J. Chem. Phys. **125**, 064506 (2006).
[7] C. Knight and S. J. Singer, J. Chem. Phys. **129**, 164513 (2008).
[8] J.-L. Kuo, M. L. Klein, and W. F. Kuhs, J. Chem. Phys. **123**, 134505 (2005).
[9] G. E. Lindberg and F. Wang, J. Phys. Chem. B **112**, 6436 (2008).
[10] A. K. Soper, Chem. Phys. **258**, 121 (2000).
[11] J. E. Bertie and J. Whalley, J. Chem. Phys. **40**, 1638 (1964).
[12] T. C. Sivakumar, S. A. Rice, and M. G. Sceats, J. Chem. Phys. **69**, 3468 (1978).
[13] M. S. Bergren, D. Schuh, M. G. Sceats, and S. A. Rice, J. Chem. Phys. **69**, 3477 (1978).
[14] P. Wong and E. Whalley, J. Chem. Phys. **62**, 2418 (1975).
[15] J. G. Scherer and R. G. Snyder, J. Chem. Phys. **67**, 4794 (1977).
[16] C. Haas and D. F. Hornig, J. Chem. Phys. **32**, 1763 (1960).
[17] T. Ford and M. Falk, Can. J. Chem. **46**, 3579 (1968).
[18] J. E. Bertie, H. J. Labbé, and E. Whalley, J. Chem. Phys. **50**, 4501 (1969).
[19] J. P. Devlin, J. Chem. Phys. **90**, 1322 (1989).
[20] A. F. Goncharov, V. V. Struzhkin, H. Mao, and R. J. Hemley, Phys. Rev. Lett. **83**, 1998 (1999).
[21] H.-C. Chang, K.-H. Huang, Y.-L. Yeh, and S. H. Lin, Chem. Phys. Lett. **326**, 93 (2000).
[22] C. G. Salzmann, A. Hallbrucker, J. L. Finney, and E. Mayer, Chem. Phys. Lett. **429**, 469 (2006).
[23] D. Eisenberg and W. Kauzmann, *The Structure and Properties of Water* (Oxford University Press, New York, 1969).
[24] *Water: A Comprehensive Treatise*, edited by F. Franks (Plenum, New York, 1972), Vol. 1.
[25] E. Whalley, Can. J. Chem. **55**, 3429 (1977).
[26] R. McGraw, W. Madden, M. Bergren, and S. Rice, J. Chem. Phys. **69**, 3483 (1978).
[27] M. J. Wójcik, K. Szczeponek, and S. Ikeda, J. Chem. Phys. **117**, 9850 (2002).
[28] V. Buch and J. P. Devlin, J. Chem. Phys. **110**, 3437 (1999).
[29] R. McGraw, W. G. Madden, S. A. Rice, and M. G. Sceats, Chem. Phys. Lett. **48**, 219 (1977).
[30] M. S. Bergren and S. A. Rice, J. Chem. Phys. **77**, 583 (1982).
[31] V. Buch, T. Tarbuck, G. L. Richmond, H. Groenzin, I. Li, and M. J. Schultz, J. Chem. Phys. **127**, 204710 (2007).
[32] M. Wojcik, V. Buch, and J. Devlin, J. Chem. Phys. **99**, 2332 (1993).
[33] J. L. Skinner, B. M. Auer, and Y.-S. Lin, Adv. Chem. Phys. **142**, 59 (2009).
[34] W. Chen, M. Sharma, R. Resta, G. Galli, and R. Car, Phys. Rev. B **77**, 245114 (2008).
[35] J. L. F. Abascal, E. Sanz, R. G. Fernàndez, and C. Vega, J. Chem. Phys. **122**, 234511 (2005).
[36] C. Vega, J. L. F. Abascal, E. Sanz, L. G. MacDowell, and C. McBride, J. Phys.: Condens. Matter **17**, S3283 (2005).
[37] J. Hayward and J. Reimers, J. Chem. Phys. **106**, 1518 (1997).
[38] C. Lee, D. Vanderbilt, K. Laasonen, R. Car, and M. Parrinello, Phys. Rev. B **47**, 4863 (1993).
[39] J. Li, J. Phys. Chem. B **101**, 6237 (1997).
[40] C. J. Burnham, J.-C. Li, and M. Leslie, J. Phys. Chem. B **101**, 6192 (1997).
[41] A. Putrino and M. Parrinello, Phys. Rev. Lett. **88**, 176401 (2002).
[42] R. Iftimie and M. E. Tuckerman, J. Chem. Phys. **122**, 214508 (2005).
[43] D. Hsu and J. L. Skinner, J. Chem. Phys. **81**, 1604 (1984).
[44] D. Hsu and J. L. Skinner, J. Chem. Phys. **81**, 5471 (1984).
[45] D. Hsu and J. L. Skinner, J. Chem. Phys. **83**, 2097 (1985).
[46] D. Hsu and J. L. Skinner, J. Chem. Phys. **83**, 2107 (1985).
[47] D. Hsu and J. L. Skinner, J. Chem. Phys. **87**, 54 (1987).
[48] J. L. Skinner and D. Hsu, Adv. Chem. Phys. **65**, 1 (1986).
[49] J. L. Skinner and W. E. Moerner, J. Phys. Chem. **100**, 13251 (1996).
[50] J. L. Skinner and D. Hsu, J. Phys. Chem. **90**, 4931 (1986).
[51] J. L. Skinner, Annu. Rev. Phys. Chem. **39**, 463 (1988).
[52] D. L. Orth, R. J. Mashl, and J. L. Skinner, J. Phys.: Condens. Matter **5**, 2533 (1993).
[53] C. P. Lawrence and J. L. Skinner, Chem. Phys. Lett. **369**, 472 (2003).
[54] C. P. Lawrence and J. L. Skinner, J. Chem. Phys. **117**, 8847 (2002).
[55] C. P. Lawrence and J. L. Skinner, J. Chem. Phys. **118**, 264 (2003).
[56] A. Piryatinski, C. P. Lawrence, and J. L. Skinner, J. Chem. Phys. **118**, 9664 (2003).
[57] A. Piryatinski, C. P. Lawrence, and J. L. Skinner, J. Chem. Phys. **118**, 9672 (2003).
[58] R. Rey, K. B. Møller, and J. T. Hynes, J. Phys. Chem. A **106**, 11993 (2002).
[59] K. B. Møller, R. Rey, and J. T. Hynes, J. Phys. Chem. A **108**, 1275 (2004).
[60] D. Laage and J. T. Hynes, Chem. Phys. Lett. **433**, 80 (2006).
[61] D. Laage and J. T. Hynes, J. Phys. Chem. B **112**, 14230 (2008).
[62] C. J. Fecko, J. D. Eaves, J. J. Loparo, A. Tokmakoff, and P. L. Geissler, Science **301**, 1698 (2003).
[63] J. D. Eaves, A. Tokmakoff, and P. L. Geissler, J. Phys. Chem. A **109**,

9424 (2005).
[64] E. Harder, J. D. Eaves, A. Tokmakoff, and B. J. Berne, Proc. Natl. Acad. Sci. U.S.A. **102**, 11611 (2005).
[65] K. Hermansson, S. Knuts, and J. Lindgren, J. Chem. Phys. **95**, 7486 (1991).
[66] T. Hayashi, T. la Cour Jansen, W. Zhuang, and S. Mukamel, J. Phys. Chem. A **109**, 64 (2005).
[67] J. R. Schmidt, S. T. Roberts, J. J. Loparo, A. Tokmakoff, M. D. Fayer, and J. L. Skinner, Chem. Phys. **341**, 143 (2007).
[68] S. A. Corcelli, C. P. Lawrence, and J. L. Skinner, J. Chem. Phys. **120**, 8107 (2004).
[69] B. Auer, R. Kumar, J. R. Schmidt, and J. L. Skinner, Proc. Natl. Acad. Sci. U.S.A. **104**, 14215 (2007).
[70] S. A. Corcelli and J. L. Skinner, J. Phys. Chem. A **109**, 6154 (2005).
[71] J. R. Schmidt, S. A. Corcelli, and J. L. Skinner, J. Chem. Phys. **123**, 044513 (2005).
[72] B. Auer and J. L. Skinner, J. Chem. Phys. **128**, 224511 (2008).
[73] B. Auer and J. L. Skinner, Chem. Phys. Lett. **470**, 13 (2009).
[74] D. E. Moilanen, E. E. Fenn, Y.-S. Lin, J. L. Skinner, B. Bagchi, and M. D. Fayer, Proc. Natl. Acad. Sci. U.S.A. **105**, 5295 (2008).
[75] B. Auer and J. L. Skinner, J. Chem. Phys. **129**, 214705 (2008).
[76] B. Auer and J. L. Skinner, J. Phys. Chem. B **113**, 4125 (2009).
[77] Y.-S. Lin, B. M. Auer, and J. L. Skinner, J. Chem. Phys. **131**, 144511 (2009).
[78] S. Mukamel, *Principles of Nonlinear Optical Spectroscopy* (Oxford University Press, New York, 1995).
[79] C. Vega, E. Sanz, and J. L. F. Abascal, J. Chem. Phys. **122**, 114507 (2005).
[80] C. Vega, M. Martin-Conde, and A. Patrykiejew, Mol. Phys. **104**, 3583 (2006).
[81] J. L. F. Abascal and C. Vega, J. Chem. Phys. **123**, 234505 (2005).
[82] R. Kumar and J. L. Skinner, J. Phys. Chem. B **112**, 8311 (2008).
[83] F. Li and C. Tainter (unpublished).
[84] D. A. McQuarrie, *Statistical Mechanics* (Harper and Row, New York, 1976).
[85] H. J. C. Berendsen, J. R. Grigera, and T. P. Straatsma, J. Phys. Chem. **91**, 6269 (1987).
[86] M. J. Frisch, G. W. Trucks, and H. B. Schlegel *et al.*, GAUSSIAN 03, Gaussian Inc., Pittsburgh, PA, 2003.
[87] D. Colbert and W. H. Miller, J. Chem. Phys. **96**, 1982 (1992).
[88] W. S. Benedict, N. Gailar, and E. K. Plyler, J. Chem. Phys. **24**, 1139 (1956).
[89] F. Paesani, S. S. Xantheas, and G. A. Voth, J. Phys. Chem. B **113**, 13118 (2009).
[90] M. P. Ljungberg, A. P. Lyubartsev, A. Nilsson, and L. G. M. Pettersson, J. Chem. Phys. **131**, 034501 (2009).
[91] A. Belch and S. Rice, J. Chem. Phys. **78**, 4817 (1983).
[92] J. E. Bertie, B. F. Francis, and J. R. Scherer, J. Chem. Phys. **73**, 6352 (1980).
[93] A. Morita and J. T. Hynes, Chem. Phys. **258**, 371 (2000).
[94] A. Morita and S. Kato, J. Chem. Phys. **110**, 11987 (1999).
[95] D. van der Spoel, E. Lindahl, B. Hess, A. R. van Buuren, E. Apol, P. J. Meulenhoff, D. P. Tieleman, A. L. T. M. Sijbers, K. A. Feenstra, R. van Drunen *et al.*, GROMACS User Manual version 3.3, www.gromacs.org, 2005.
[96] T. Darden, D. York, and L. Pedersen, J. Chem. Phys. **98**, 10089 (1993).
[97] U. Essmann, L. Perera, M. L. Berkowitz, T. Darden, H. Lee, and L. G. Pedersen, J. Chem. Phys. **103**, 8577 (1995).
[98] S. Miyamoto and P. A. Kollman, J. Comput. Chem. **13**, 952 (1992).
[99] M. F. Kropman, H.-K. Nienhuys, S. Woutersen, and H. J. Bakker, J. Phys. Chem. A **105**, 4622 (2001).
[100] R. Laenen, K. Simeonidis, and A. Laubereau, J. Phys. Chem. B **106**, 408 (2002).
[101] J. C. Deàk, L. K. Iwaki, S. T. Rhea, and D. D. Dlott, J. Raman Spectrosc. **31**, 263 (2000).
[102] J. D. Smith, C. D. Cappa, K. R. Wilson, R. C. Cohen, P. L. Geissler, and R. J. Saykally, Proc. Natl. Acad. Sci. U.S.A. **102**, 14171 (2005).
[103] S. Woutersen, U. Emmerichs, H.-K. Nienhuys, and H. J. Bakker, Phys. Rev. Lett. **81**, 1106 (1998).
[104] R. Laenen, C. Rauscher, and A. Laubereau, Phys. Rev. Lett. **80**, 2622 (1998).
[105] G. M. Gale, G. Gallot, F. Hache, N. Lascoux, S. Bratos, and J.-C. Leicknam, Phys. Rev. Lett. **82**, 1068 (1999).
[106] H.-K. Nienhuys, S. Woutersen, R. A. van Santen, and H. J. Bakker, J. Chem. Phys. **111**, 1494 (1999).
[107] G. M. Gale, G. Gallot, and N. Lascoux, Chem. Phys. Lett. **311**, 123 (1999).
[108] C. J. Fecko, J. J. Loparo, S. T. Roberts, and A. Tokmakoff, J. Chem. Phys. **122**, 054506 (2005).
[109] H. Iglev, M. Schmeisser, K. Simeonidas, A. Thaller, and A. Laubereau, Nature (London) **439**, 183 (2006).
[110] H. Bakker and J. L. Skinner, Chem. Rev. (Washington, D.C.) **110**, 1498 (2010).
[111] R. Kubo, Adv. Chem. Phys. **15**, 101 (1969).
[112] B. Auer and J. L. Skinner, J. Chem. Phys. **127**, 104105 (2007).
[113] J. R. Schmidt, N. Sundlass, and J. L. Skinner, Chem. Phys. Lett. **378**, 559 (2003).
[114] H. Tanaka, J. Mol. Liq. **90**, 323 (2001).
[115] A. R. Henn and W. Kauzmann, J. Phys. Chem. **93**, 3770 (1989).
[116] C. P. Lawrence and J. L. Skinner, J. Chem. Phys. **117**, 5827 (2002).
[117] F. Li and J. L. Skinner, "IR and Raman line shapes for ice Ih. II. H_2O and D_2O," J. Chem. Phys. (to be published).
[118] J. B. Asbury, T. Steinel, C. Stromberg, S. A. Corcelli, C. P. Lawrence, J. L. Skinner, and M. D. Fayer, J. Phys. Chem. A **108**, 1107 (2004).